

High-Strength Dissimilar Welds Between a NiTi Shape Memory Alloy and Titanium Obtained by Intermixing Niobium Using Pulsed Laser Beam Welding



M. WIEGAND , N. SOMMER , L. MARKS, and S. BÖHM

Joining of NiTi shape memory alloys with commercially pure titanium (Ti) is of great interest for manifold industrial applications. However, dissimilar fusion welding of these materials is associated with the formation of extremely brittle intermetallic compounds, *e.g.*, Ti_2Ni and $TiNi_3$, which drastically limit the mechanical properties of NiTi/Ti joints. The present investigation seeks to improve both chemical compatibility and mechanical performance through intermixing of a niobium foil as filler material into a NiTi/Nb/Ti butt-joint configuration by means of pulsed laser beam welding. Different pulse durations are applied to tailor intermixing and evaluate the deviating chemical compositions of the weld metal. It is demonstrated that intermixing of niobium significantly increases the weldability of the material combination NiTi/Ti compared to autogenous welding. However, the proportion of intermixed filler material exerts a substantial impact on the microstructural evolution and mechanical properties. Ultimate tensile strengths of up to 679 MPa with fracture occurring in the titanium base metal at an elongation at break of 18.7 pct is obtained by a reduction of the pulse duration, which represents a major improvement over previous studies focusing on fusion welding of NiTi to titanium and its alloys.

<https://doi.org/10.1007/s11661-023-07248-w>

© The Author(s) 2023

I. INTRODUCTION AND STATE-OF-THE-ART

A. Dissimilar Welding of Nickel-Titanium Alloys

NICKEL-TITANIUM shape memory alloys (NiTi) are applied in a wide range of modern applications including medical technologies, aerospace, energy generation, and various other industrial sectors.^[1–6] This can be attributed to their unique properties, namely the temperature-induced shape memory effect as well as excellent superelasticity, depending on the composition of the material. Superelastic alloys, as for example grade SE 508, can achieve high elastic deformations of up to 8 pct at stress levels between 400 and 500 MPa.^[7] In addition, NiTi-alloys are characterized by excellent

corrosion resistance and biocompatibility.^[3,8] However, the comparatively high price as well as poor machinability restrains a wider usage in mass-produced and large-scale products. To counteract such material-specific disadvantages, dissimilar welding is a promising approach, as the combination of individual material properties in optimized and graded parts can lead to enhanced functional, manufacturing and economic advantages.^[9,10] Owing to this, dissimilar welding has become increasingly relevant for scientific and industrial efforts in recent years, as exemplified by multiple investigations on NiTi/stainless steel,^[11] copper/stainless steel,^[12,13] and copper/aluminum.^[14]

Especially titanium (Ti) and its alloys are promising materials for dissimilar joining with NiTi, as they share excellent corrosion resistance and biocompatibility while providing great mechanical properties, *e.g.*, a high strength-to-density ratio and can consequently be used in similar application areas.^[15–17] However, dissimilar fusion welding of Ti to NiTi is associated with various challenges due to pronounced chemical incompatibilities and thermophysical differences of the two materials. Joining is mainly restricted by a very low solubility in solid state as well as the formation of extremely brittle, ceramic-like intermetallic compounds (IMC), for instance, Ti_2Ni and $TiNi_3$.^[18] These IMC are formed

M. WIEGAND, N. SOMMER, S. BÖHM are with the Department for Cutting and Joining Manufacturing Processes, Institute for Production Technologies and Logistics, University of Kassel, Kurt-Wolters-Str. 3, 34125 Kassel, Germany. Contact e-mail: m.wiegand@uni-kassel.de. L. MARKS is with the NMI Natural and Medical Sciences Institute at the University of Tübingen, Markwiesenstr. 55, 72770 Reutlingen, Germany.

Manuscript submitted April 3, 2023; accepted October 27, 2023.

Article published online November 17, 2023

in a wide range of chemical compositions and strongly affect the weldability and mechanical properties of the obtained joints. Moreover, the deviating thermophysical properties of the materials, such as melting temperatures, thermal conductivities, and thermal expansion rates, can further increase the susceptibility to cracking upon solidification.^[19,20]

Nevertheless, an implementation of this material combination by means of fusion welding processes, such as laser or electron beam welding, is desirable for many industrial applications, as these processes allow a very high freedom of design compared to pressure welding processes or form- and force-fit joining methods. Consequently, the joining of small and complex geometries, *e.g.*, parts with an application in the medical sector, is possible. Furthermore, precise control of beam welding process parameters can lead to improved heating and cooling rates and, thus, small weld pool sizes as well as heat-affected zones (HAZ) can be generated. By means of micro beam welding technologies with a correspondingly small focus diameter, the component and joint size can be miniaturized to a greater extent. By utilizing these advantages, the adverse effects of the thermophysical differences can be drastically reduced, making beam welding processes very promising for dissimilar welding.^[21]

B. State-of-the-Art in Dissimilar Beam Welding of Nickel-Titanium to Titanium

According to the aforementioned high scientific and industrial interest in dissimilar beam welding of NiTi, a multitude of authors have investigated the joining to Ti with a major focus on laser beam welding. Their findings will be briefly summarized in the following.

Shojaei Zoeram and Akbari Mousavi^[20] as well as Miranda *et al.*^[22] investigated autogenous laser beam welding of Ti6Al4V to NiTi with a pulsed Nd:YAG laser and a Yb fiber laser, respectively. In both studies, no durable joints were produced due to direct failure of the weld metal resulting from the formation of Ti₂Ni IMC. Datta *et al.*^[19] came to analogous conclusions and observed strong solidification cracking upon direct joining of Ti to NiTi without filler materials which were attributed to IMC formation and the associated high hardness values in the weld seams. These investigations pinpoint that an implementation of filler materials is expedient for fusion welding of Ti to NiTi in order to improve the chemical compatibility and, thus, the weldability and mechanical properties.

In accordance with this conclusion, several investigations with different filler materials for the Ti/NiTi dissimilar joint were conducted. Consequently, it could be demonstrated that it is possible to obtain a significant increase of joint quality by the use of a copper interlayer, leading to tensile strengths up to 300 MPa.^[20] Investigations by Teshome *et al.* revealed that the implementation of zirconium^[23] or cobalt^[24] interlayers in combination with a beam offset on the Ti-side of the joint reduces the hardness values and considerably improves the mechanical performance

compared to autogenous welding, reaching strength values of 320 and 285 MPa, respectively. Within a very recent study by Teshome *et al.*,^[25] the achievable mechanical properties were further increased to 520 MPa tensile strength by the use of a palladium interlayer. However, the fracture of the corresponding specimens remains in the fusion zone, thus still representing a weak point.

Another promising filler material for the joining of Ti and NiTi is niobium (Nb), which can be attributed to the good miscibility and compatibility to the Ti base material.^[26,27] Oliveira *et al.*^[28] used Nb as a diffusion barrier between Ti6Al4V and NiTi and observed tensile strengths of up to 300 MPa. Ge *et al.*^[29] investigated laser welding of Nb in overlapping configuration between Nitinol and Ti2AlNb, proving the possibility to create sound joints capable of withstanding lap shear forces of up to 1236 N when intermixing appropriate proportions of the filler material into the weld metal. In a recent investigation, Wiegand *et al.*^[5] examined micro-electron beam welding of Ti to NiTi by applying tantalum, hafnium, and niobium as interlayers between Ti and NiTi. It was found that particularly Nb is a highly effective filler material for this material combination, as no critically high hardness values were detected in the weld seam to NiTi, despite the tendency for IMC formation between Nb and nickel (Ni). Furthermore, excellent mechanical properties were observed with tensile specimens failing inside the un-molten filler material at an average tensile strength of 453 MPa, proving the great compatibility function of Nb when welding NiTi to Ti.

II. SCOPE OF THE PRESENT INVESTIGATION

The investigation at hand builds on the previous studies and specifically addresses the intermixing of Nb foil into dissimilar joints of Ti/NiTi using a butt-welding configuration by means of pulsed laser beam welding. In order to control and evaluate deviating chemical compositions of the three materials, different weld metal geometries are generated by varying pulse durations. The resulting chemical compositions are analyzed by means of energy-dispersive X-ray spectroscopy (EDS) mappings and line scans for the samples welded with 1 and 10 ms pulse duration. In addition, a comparison of the microstructural evolution for these parameter sets was conducted using scanning electron microscopy (SEM) equipped with a secondary (SE2) and backscattered-electron detector (BSE) as well as electron backscatter diffraction (EBSD). To deduce the interrelationships of microstructural evolution and mechanical properties, tensile tests and nanoindentation mappings are performed.

The results demonstrate that a robust fabrication of defect-free joints with non-critical hardness values is feasible, leading to excellent mechanical properties. However, the latter are strongly affected by the applied pulse durations and the metallurgical influences resulting therefrom.

Table I. Chemical Composition of Titanium Grade 4 as Specified by the Material Suppliers

Element (Wt Pct)				
Ti	C	N	Fe	O
Bal.	0.011	0.010	0.12	0.31

III. MATERIALS AND METHODS

The experiments were performed using thin sheet geometries measuring 12.5 mm × 25 mm × 0.25 mm of commercially pure titanium (cp-Ti, grade 4) as well as superelastic NiTi. Tables I and II depict the chemical composition of the sheets.

As filler material, thin Nb strips measuring 12.5 mm × 0.1 mm × 0.25 mm were inserted between the abutting edges of the joint configuration. All welding specimens were produced by electrical discharge machining (EDM). The joining surfaces of the materials were ground using P2500 silicone-carbide paper to remove process related oxide-layers and impurities as well as to provide an optimal surface finish. The samples were subsequently cleaned using acetone and dried in air. To ensure optimal and reproducible welding conditions with virtually no gap, the samples were placed in a specifically designed fixture arrangement. The filler material was then held in position by applying sufficient pressure on lateral clamping jaws. Figure 1 visualizes the welding configuration in schematic form as well as the area of interest for the subsequent experiments.

Table III summarizes relevant thermophysical and mechanical properties of the materials used in this investigation.

The welding tests were performed using a pulsed Nd:YAG laser SLS 200 CL 8 (Coherent Switzerland AG, formerly ROFIN-LASAG AG, Belp, Switzerland) featuring a near-Gaussian intensity distribution as well as a wavelength of 1064 nm. The laser source enables a maximum laser output of 1 kW with the given setup. The pulse length can be regulated between 0.5 and 100 ms while the pulse frequency allows adjustments between 0.1 and 500 Hz. In addition to that, free-form pulse modulation can be performed to further control the laser power of the individual pulses.^[33] A beam guiding fiber with a diameter of 50 μm transfers the beam to an LLBK60 processing head (Coherent Switzerland AG, formerly ROFIN-LASAG AG, Belp, Switzerland), in which the beam is focussed to a diameter of approximately 38 μm by an adjustable unit consisting of a collimating and focusing lens. To provide optimal protection of the highly reactive materials, the weld seam root as well as the bead top was shielded from atmospheric influence using argon 4.8 (99.998 pct purity).

Table IV summarizes the parameters used in the experiments. The weldments were performed using varying pulse durations between 1 and 10 ms in order to produce different weld metal geometries. The peak power was adjusted for the individual pulse durations to minimize the energy input while ensuring full

penetration through the high-melting filler material. For the specimens welded with pulse durations of 1 and 3 ms, a smaller pulse interval of 0.05 mm was necessary in order to provide a sufficient binding of the metals down to the weld seam root, which was realized by a slower traverse speed of 0.15 mm/s with the constant frequency of 3 Hz. Figure 2 visualizes the employed free-form pulse modulation which was applied to ensure a more homogenous cooling.

The weld seams were analyzed with the aid of optical light microscopy (DM2700, Leica Microsystems GmbH, Wetzlar, Germany). For this purpose, the welded specimens were ground to the center of the weld, as schematically illustrated in Figure 1, using silicone-carbide paper and subsequently polished using a diamond suspension (grit size 0.1 μm). To highlight the microstructural features of Ti, a hydrofluoric-acid-free etching solution according to Keller was applied for 120 s at room temperature. Weld seam surface analyses were carried out by means of SEM (Zeiss REM Ultra Plus, Carl Zeiss AG, Oberkochen, Germany) operating at an acceleration voltage of 15 kV. The chemical gradient along the weld cross-section was examined using EDS (Bruker XFlash 6160, Bruker Corporation, MA). Dendrite formation morphologies were evaluated using SE2- and BSE imaging in the aforementioned SEM operating at an acceleration voltage of 10 kV. To highlight the grain structure of the corresponding weld seams, the specimens were etched using a mixture of 65 pct nitric acid and 38 pct hydrofluoric acid (ratio 9 to 1) for 1 second at room temperature. Moreover, the resulting grain morphologies and sizes were analyzed and compared using EBSD (Symmetry, Oxford Instruments plc, Abingdon, England) at an accelerating voltage of 10 kV. Due to considerable differences in the topographical requirements of the various metallographic analyses, they were performed on separate levels of the cross-section or partly on new, identically welded specimens. This explains the visible small deviations in the weld geometries.

Nanoindentation measurements were performed using a nanoindentation tester (NHT2, Anton Paar GmbH, Graz, Austria) with a maximum load of 10 mN and loading and unloading speeds of 100 mN/s. Tensile tests were carried out on the basis of DIN EN ISO 6892-1 with a universal testing machine (Z100, Zwick-Roell AG, Ulm, Germany) using bone-shaped tensile testing samples, which were extracted using EDM. The specimens were clamped using a preload of 5 N and subsequently tested with regard to their ultimate tensile strength and elongation at break. The mechanical properties were determined using three identically manufactured specimens for each set of parameters.

IV. RESULTS AND DISCUSSION

A. Microstructural Analyses of the Titanium/Niobium/NiTi Joints

Light microscopy analyses of the joint cross-sections depicted in Figures 3(a) through (d) confirm that

Table II. Chemical Composition of NiTi as Specified by the Material Suppliers

Element (Wt Pct)						
Ni	Ti	C	O	Fe	other single trace elements	
55.94	bal.	0.0275	0.019	0.014	< 0.01	

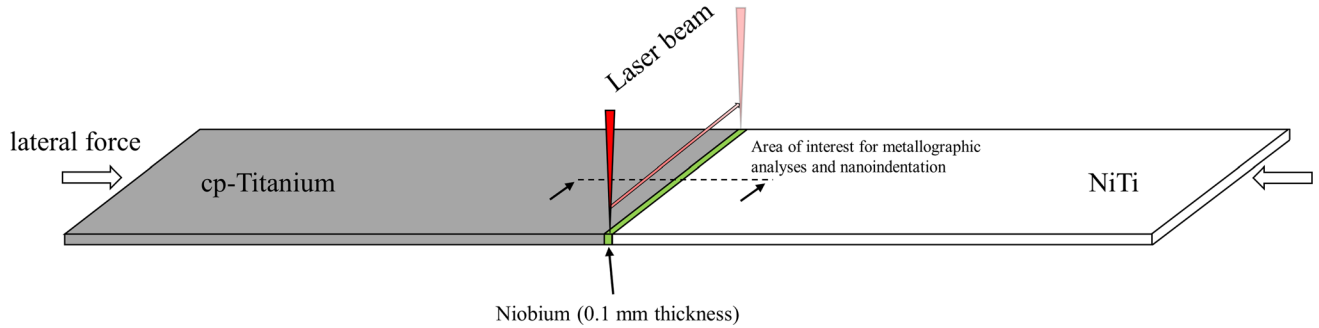


Fig. 1—Schematic illustration depicting the setup and trajectory of the welding process as well as sample extraction location.

Table III. Selected Thermophysical and Mechanical Properties of the Respective Alloys Used in this Investigation

Materials	Melting point (°C)	Ultimate Tensile Strength (MPa) *	Elongation at Break * [Pct]	Initiation Loading Plateau* [MPa]	Thermal Conductivity [$Wm^{-1} K^{-1}$]	Coefficient of Thermal Expansion [$10^{-6} K^{-1}$]
cp-Titanium (Grade 4)	1660	~ 679	~ 23	–	18	8.6
NiTi (55.8 Wt Pct Nickel)	1310	~ 1357	~ 12	~ 400	18	11
Niobium (99.9 Pct)	2468	~ 254	~ 42	–	52	7.1

All values are given for a temperature of 20 °C.^[7,30–32] The mechanical properties (*) were determined by tensile tests on the experimental material

Table IV. Overview of the Welding Parameters Used in the Investigation at Hand

Parameter	Pulse Duration (ms)	Peak Power (W)	Traverse Speed (mm/s)	Pulse Interval (mm)	Focus Position	Pulse Frequency (Hz)	Pulse Modulation
I	1	600	0.15	0.05	surface	3	“triangle”
II	3	350					
III	5	280	0.3	0.1			
IV	10	180					

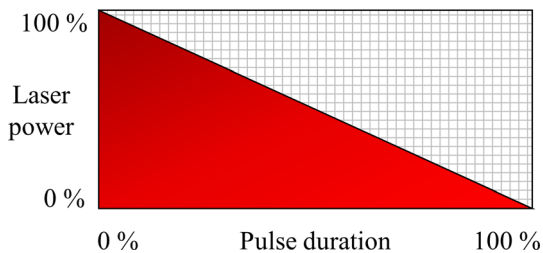


Fig. 2—Illustration of the pulse modulation “Triangle” used for welding.

strongly deviating weld geometries can be generated using the aforementioned sets of parameters. Despite the considerably differing welding intensities and energy inputs, all specimens are crack-free. This underlines a major increase of the weldability compared to autogenous welding of Ti to NiTi.^[19,20,22]

A comparison between the micrographs of the different parameter sets reveals a significant increase of the weld seam width as well as the range of the HAZ for higher pulse durations. This can be attributed to the longer interaction time of the laser beam with the material, the associated higher energy input and the

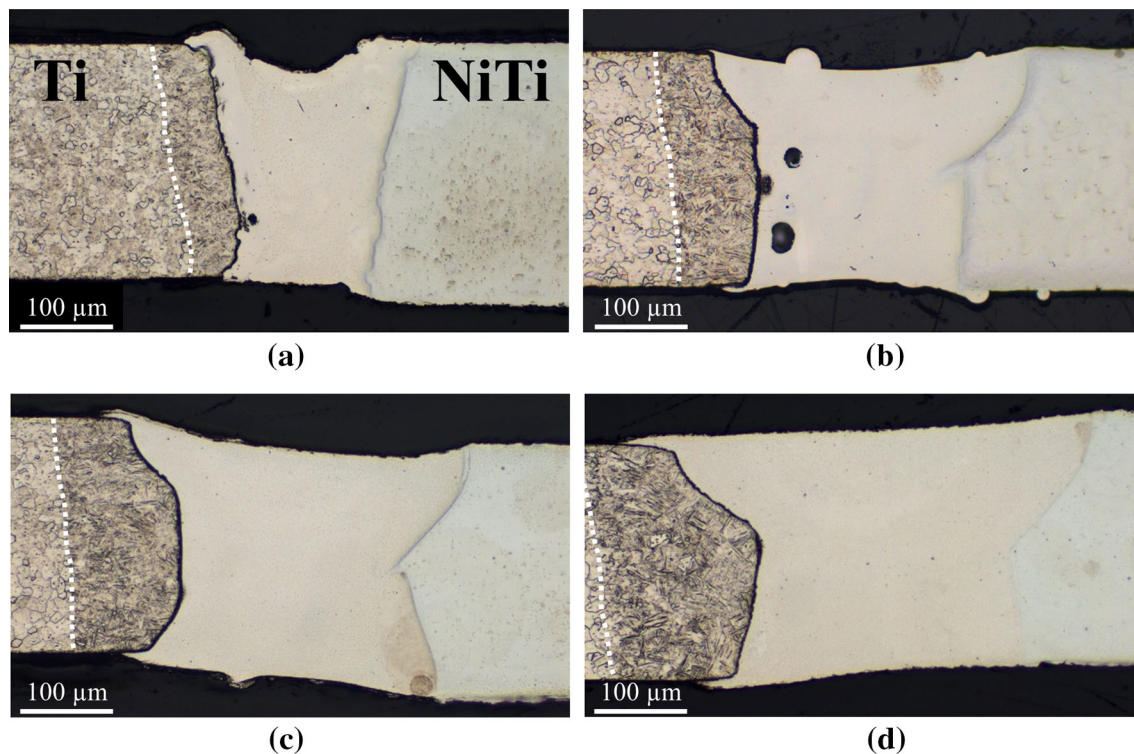


Fig. 3—Etched cross-sections of the applied parameter sets I (a), II (b), III (c), and IV (d). The dotted lines highlight the approximate range of the HAZ.

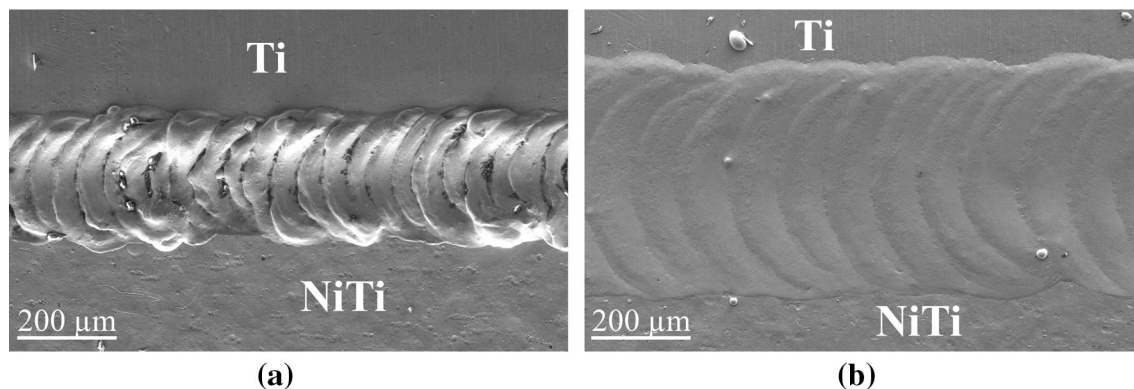


Fig. 4—SE2-images depicting the weld seam surfaces of parameter I (a) and IV (b).

increased time for heat conduction to take effect and is in good agreement with previous studies using free-form pulse shaping.^[33] Another significant feature that can be derived from Figure 3(a) is the strong undercutting for the sample welded with 1 ms pulse duration. This can be explained by the comparatively high peak power of 600 W in combination with the small focus diameter of the system, leading to excessive intensity on the workpiece surface. On the contrary, this pulse peak power is required to ensure a complete penetration of the weld seam as well as a sufficient melting and binding with the two base metals along the entire sheet thickness. With an increased pulse duration and correspondingly lower peak power required to achieve sufficient melting of all metals, this effect decreases, resulting in more

homogeneous weld seams, as can be especially seen for the sample welded with parameters III and IV in Figures 3(c) and (d). Furthermore, pores were partially observed in the weld metal of some specimens during the course of the investigation, as can be seen for example in Figure 3(b). These represent gas inclusions, which can possibly be attributed to the strongly differing melting and boiling temperatures of the base and filler materials. By optimizing the process, *e.g.*, by defocusing or by adapted pulse shaping, they could most likely be avoided.

To further illustrate the pronounced differences of the weld geometries, overviews of the weld bead surfaces of samples I and IV were obtained by means of SEM. As can be observed for the sample welded with 1 ms pulse

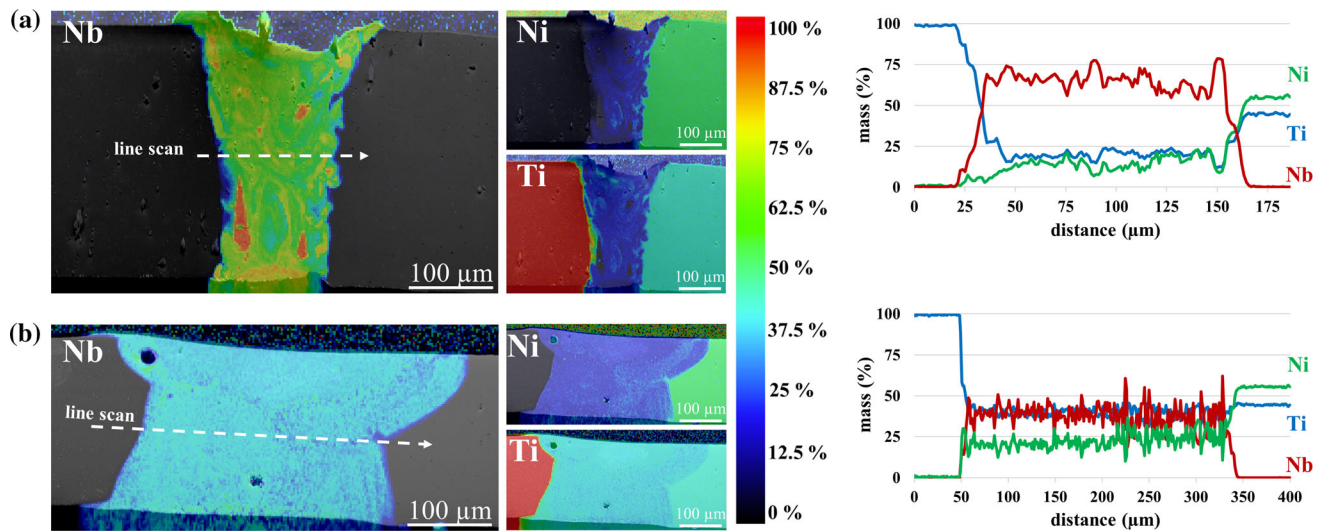


Fig. 5—EDS mappings and corresponding line scans for Nb, Ni & Ti, obtained along cross-sections of parameter set I (a) and IV (b).

duration in Figure 4(a), the weld metal is partly expelled from the weld seam, resulting in a high topography and the aforementioned undercutting in the center of the weld seam. The irregularities clearly exist across multiple pulses along the course of the weld seam and can be attributed to an increased vapor pressure as a result of the previously mentioned very high intensity of this parameter set. In addition, focus shifts due to the expelled weld metal are likely, leading to the apparent high turbulence of the process and the resulting uneven weld seam formation. In contrast to this, only minimal topography is visible for the specimen welded with a pulse duration of 10 ms in Figure 4(b). Consequently, the solidified weld metal shows a much higher uniformity along the displayed weld bead surface, compared to parameter set I.

The main objective of applying different beam pulse durations was to achieve deviating chemical compositions, as this feature is anticipated to have a decisive influence on the overall weld seam properties. By generating narrow weld seams, the proportion of Nb filler material within the weld metal is expected to be correspondingly high, whereas more of the base materials should be intermixed as the weld seam width increases. In order to evaluate the interrelationship between the pulse durations and the compositions, EDS mappings and line scans were performed on the samples welded with parameter I and IV. As can be derived by the phase mappings in Figure 5(a), fragments of un-molten Nb filler material can be identified in the weld seam of the sample welded with parameter set I. As discussed before, the required high peak power leads to strong turbulence and welding irregularities, which may be the root cause for uneven melting. Another possible explanation for this inhomogeneity is the pulsed laser beam welding process itself. While a complete penetration and melting of the filler material is to be expected in the center of a pulse, a lower power input is exerted in the overlapping area between two pulses. The analyzed cross-section may represent a plane of the specimen in

such an area, which in turn could explain the uneven melting of the comparatively high-melting filler material. In the remaining weld seam, the distribution of the individual materials is found to be rather homogeneous. However, increased concentrations of Ti and Ni can be detected at their respective fusion lines adjacent to the Ti and NiTi base materials. A uniform mixing of the materials does consequently not fully occur with this parameter set. The corresponding line scan confirms a high amount of Nb inside the weld metal, averaging at approximately 60 pct along the cross-section. This can be attributed to the fact that the weld seam is only slightly wider than the Nb foil, which has a thickness of 100 μm .

In comparison, the EDS mappings of the sample welded with parameter set IV and 10 ms pulse duration prove a strongly increased homogeneity with respect to the intermixing of the three materials, compared to parameter set I. There are no un-molten parts of the filler material detectable and the material distribution in the range of the fusion lines is also of much higher uniformity. This can be explained by the significantly longer interaction time between the beam and the material leading to a longer timeframe in the liquid phase. As a result, intermixing processes have more time to take effect. As expected, the Nb content of parameter IV is significantly lower due to the much wider weld seam width, leading to an increased intermixing of the base materials. The line scan reveals that the content of Nb is comparable to Ti inside the weld metal and averages at approximately 37 pct, thus significantly lower compared to parameter set I.

In order to obtain a comparison of the resulting microstructural evolution arising from the identified deviating chemical compositions, identically welded specimens of parameter I and IV were etched and subsequently examined by SEM and BSE analyses. Based on the SEM images in Figures 6(a) through (d), the previous findings for the solidification of both samples can be confirmed, as un-molten fragments of

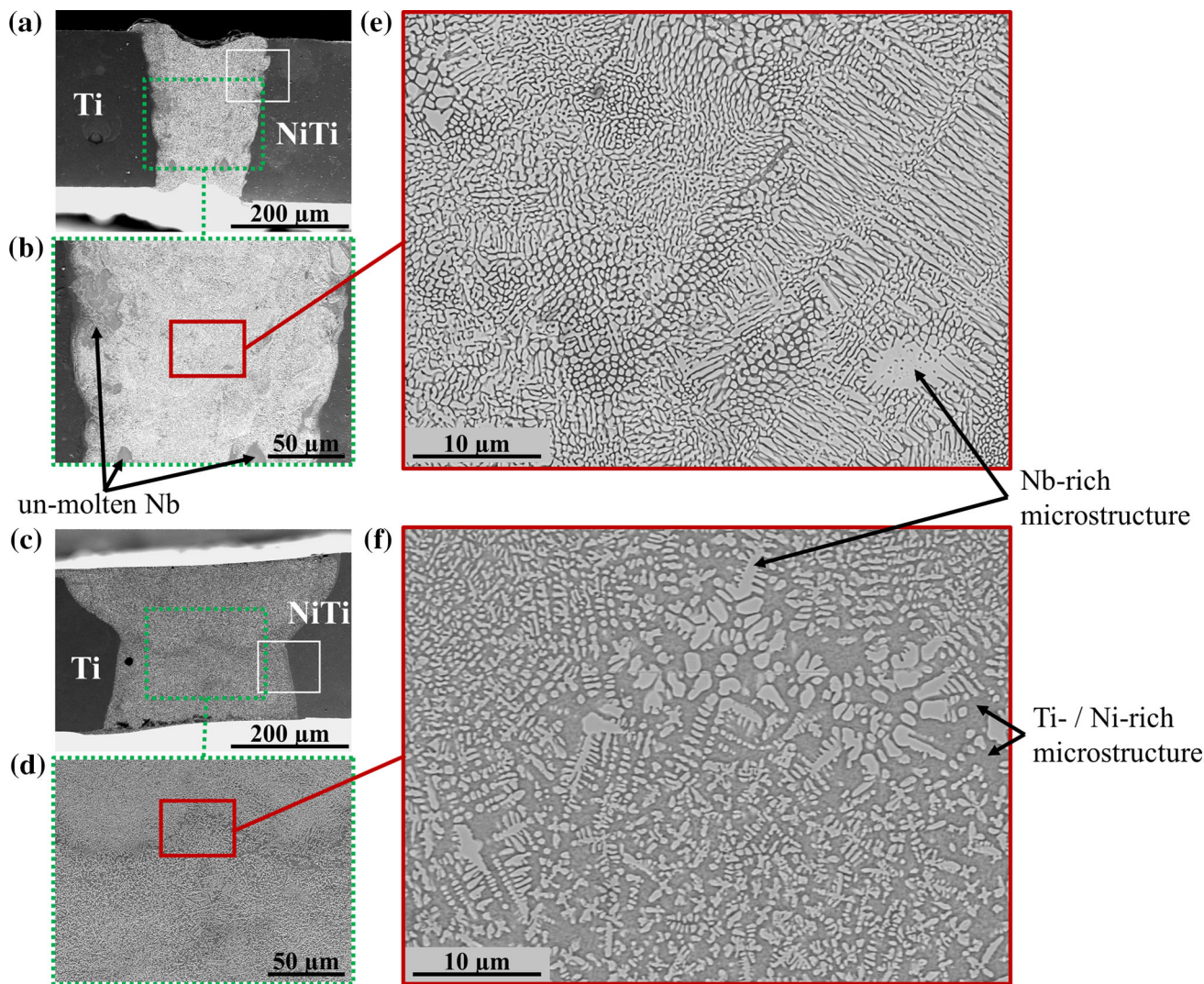


Fig. 6—SE2-images visualizing the microstructure of etched cross-sections welded with parameter I (a, b) and IV (c, d). (e) and (f) depict BSE images of the indicated regions. The white rectangles in (a) and (b) mark the areas of interest for the subsequent EDS and EBSD analyses in Figs. 7 and 8.

the Nb filler material can be identified for parameter I, while parameter IV shows a high uniformity. However, both samples are characterized by a fine dendritic microstructure in the intermixed areas.

The BSE images, which were obtained in representative areas in the center of the specimens, confirm substantial differences in the resulting microstructure of the two parameter sets, as can be seen by a comparison of Figures 6(e) and (f). Based on the material contrast, which correlates with the different atomic numbers,^[34] parameter I shows a predominant development of Nb-rich dendritic structures. Identical dendrites can also be identified for parameter IV, although in a significantly smaller area fraction. The dark interdendritic microstructure, which is much more pronounced for parameter IV compared to parameter I, represents Ti- and Ni-rich phases.

These observations were further validated by subsequent EDS mappings, generated in the transition area between the weld seams and the NiTi base material, as

highlighted in Figures 6(a) and (c). The chemical characterization proves a distinct enrichment of Nb in the dendritic microstructure. Furthermore, it can be observed that Ti is distributed rather homogeneously inside the weld metal, whereas Ni is noticeably more present in interdendritic areas. This is particularly evident in Figure 7(b) for parameter set IV. This observation can be explained by the different solubility of the materials. While Ti has very good miscibility with Nb and consequently forms solid solutions with the filler material, the solubility of Ni in Nb is strongly limited,^[35] which in turn explains the clearly deviating proportion of the materials in the dendritic structure.

Based on the BSE and EDS analyses, it can be anticipated that IMC of the type Ti_2Ni , which are considered highly critical based on previous studies,^[19,20,22] are present within the Ni- and Ti-rich interdendritic regions and, thus, substantially more pronounced in parameter IV. This correlates with previous studies, as an accumulation of Ti_2Ni in

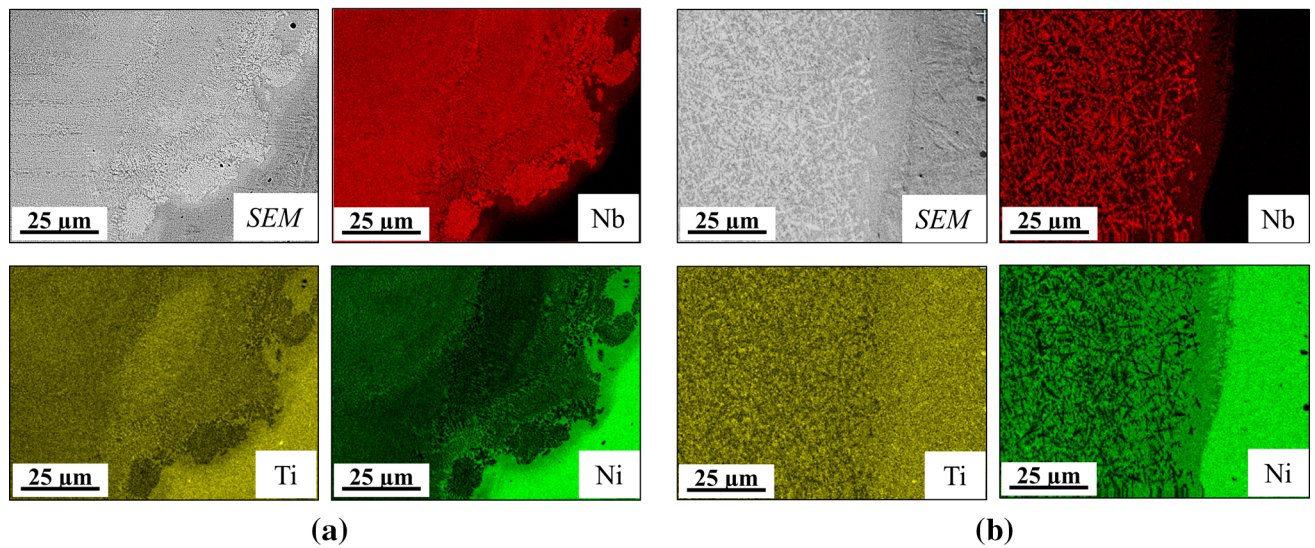


Fig. 7—SE2-images and EDS mappings of parameter I (a) and IV (b) highlighting the material distribution within the dendritic and interdendritic microstructure. Areas of interest as marked in Fig. 6.

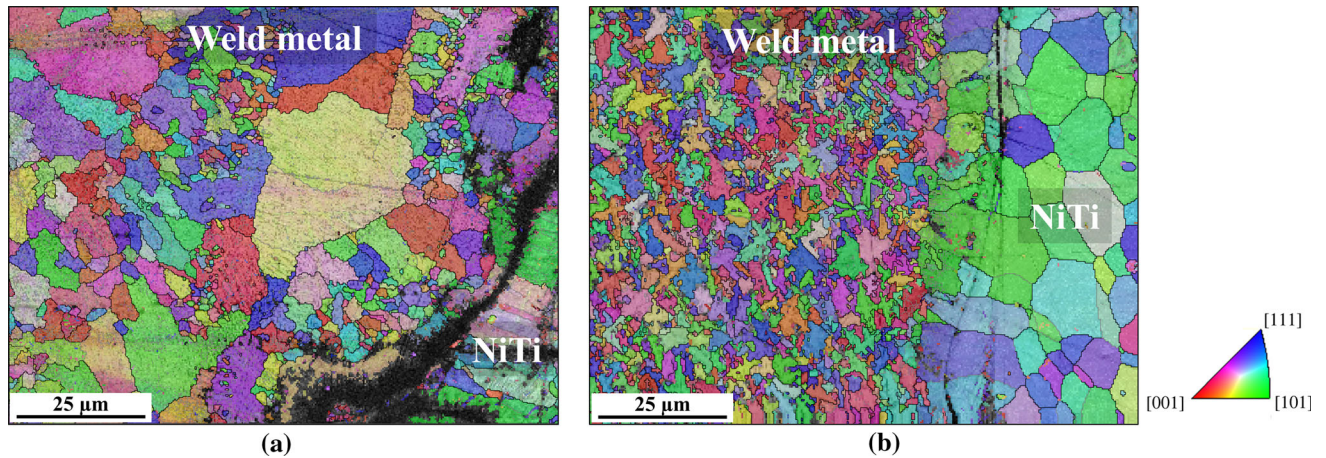


Fig. 8—Superimposed image quality mapping and inverse pole figure mapping of parameter I (a) and IV (b). Areas of interest are identical to Fig. 7.

interdendritic regions was also reported by Miranda *et al.*^[22]

In order to conclude the microstructural analyses, the grain morphologies of the previously examined parameter sets I and IV were examined by means of EBSD in identical areas as Figures 7(a) and (b). As can be derived from Figure 8, the two parameter sets show strong differences in the resulting grain morphology. As for parameter I, it can be observed that the previously identified fine dendritic structure partially accumulates into comparatively large grains. However, the grain sizes are also present in a bimodal distribution, as both very fine-grained structures and comparatively coarse-grained areas are present within the weld seam. This uneven distribution can again be attributed to the previously mentioned high melt pool turbulence of this parameter set, which in turn cause strong intermixing gradients. Consequently, local differences in the

thermophysical properties can be expected, which certainly have a high influence on the resulting microstructure and grain size formation. In addition, the analysis of parameter set I is associated with poor band contrast along the fusion line, represented by the black areas. These can be attributed to locally pronounced lattice distortion and indicate increased stresses in the weld metal. Parameter IV is again characterized by a high uniformity inside the weld seam. Despite a prolonged pulse duration and, consequently, a longer timeframe in the molten phase and slower cooling rates, parameter IV exhibits a significantly finer-grained microstructure overall compared to parameter set I. This effect can be related to the strongly differing chemical composition due to the reduced amount of Nb in the weld metal. The more homogeneous mixing of the three materials may also contribute to a uniform phase separation, inevitably resulting from the low miscibility of the materials.

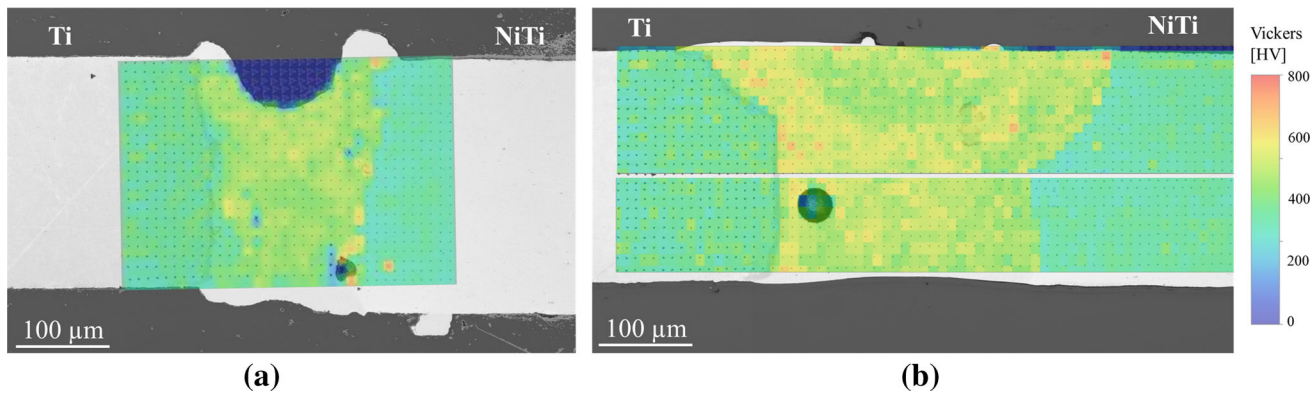


Fig. 9—Nanoindentation mappings across the cross-sectional area of samples welded with parameter set I (a) and parameter set IV (b).

It should be noted at this point that it was not feasible to precisely identify the present phases using the EBSD method. This is due to the large number of possible IMC,^[36] which cannot be distinguished based on similar lattice parameters. In addition, due to the extreme cooling rates and the inhomogeneous mixing conditions, it can be assumed that no equilibrium states prevail. While the investigation at hand provides an in-depth analysis of the microstructural evolution of this dissimilar material combination, further studies with extensive phase analyses using transmission electron microscopy or X-ray diffraction should be carried out to completely understand the complex solidification mechanisms.

In summary, the microstructural analyses confirm that the various pulse durations and weld seam geometries lead to drastic differences in the resulting chemical compositions as well as the microstructural evolution. It can be concluded that a narrow weld seam, as generated by parameter set I, is associated with the formation of a Nb-rich microstructure resulting from a higher proportion of filler metal in the weld metal. However, strong macroscopic and microscopic irregularities were also detected for this parameter set. Longer pulse durations and wider weld seams, on the other hand, lead to a higher proportion of Ti and Ni in the weld, which in turn increases the size of interdendritic microstructures. The weld seams are also significantly more uniform due to less melt pool turbulence and prolonged timeframes for intermixing processes to take effect.

B. Mechanical Properties of the Titanium/Niobium/NiTi Joints

For dissimilar welding of only limitedly miscible materials with a tendency to IMC formation, the hardness of the joint is of crucial importance for the weldability and mechanical resilience of the joint. High concentrations of IMC and the associated high hardness peaks can act as drastic weak points under stress.^[5] Based thereon, a detailed nanoindentation mapping of both the samples welded with parameter set I and IV was performed, as depicted in Figures 9(a) and (b). For parameter set I, an increase in hardness inside the weld seam compared to the base materials can be observed. However, the average hardness of approximately 550

HV within the weld seam is relatively low compared to autogenous welding of Ti and NiTi, for which over 1000 HV were reported.^[22] This indicates that the addition of Nb into the weld metal is associated with a reduced amount of critical IMC. Parameter set IV shows comparable results; however, the overall hardness is noticeably higher compared to the narrow weld seam of parameter set I. In addition, occasional hardness peaks above 700 HV can be observed. The considerable differences in chemical composition, especially the lower Nb content in the weld seam for parameter set IV and the higher concentration of Ti- and Ni-rich phases at the interdendritic spaces, clearly lead to increased hardness values compared to parameter I. This confirms the previously established assumption, that the increased presence of Ni- and Ti-rich interdendritic microstructure resulting from enlarged intermixing promotes the formation of hard IMC, such as Ti_2Ni .

To correlate the previous findings to the mechanical performance, tensile tests for each of the four parameter sets were performed. As can be derived from Figure 10(a), the pulse duration and the associated metallurgic differences discussed in the previous section have a significant influence on the ultimate mechanical properties. Consequently, samples welded with 1 ms pulse duration excel with very high ultimate tensile strengths and fracture elongations. It shall be particularly emphasized that a majority of these specimens have in fact failed in the Ti base material at approximately 679 MPa ultimate tensile strength and, thus, outside the welding area, as shown in Figure 10(b). The premature failure of one of the specimens can be attributed to the above-mentioned, partly severe irregularities in the weld geometries as well as the inconsistent melting of the high-melting Nb. In comparison with parameter set I, a continuous decrease of the average ultimate tensile strength as well as elongation at break can be observed by increasing the pulse duration up to 5 ms. However, when the pulse duration is further increased to 10 ms, the mechanical performance remains similar to the one observed at a pulse duration of 5 ms. The reduction in tensile strength for longer pulse durations and wider weld seams is in good agreement with the observed increased hardness values in the weld metals. The prolongation of the pulse duration and the associated

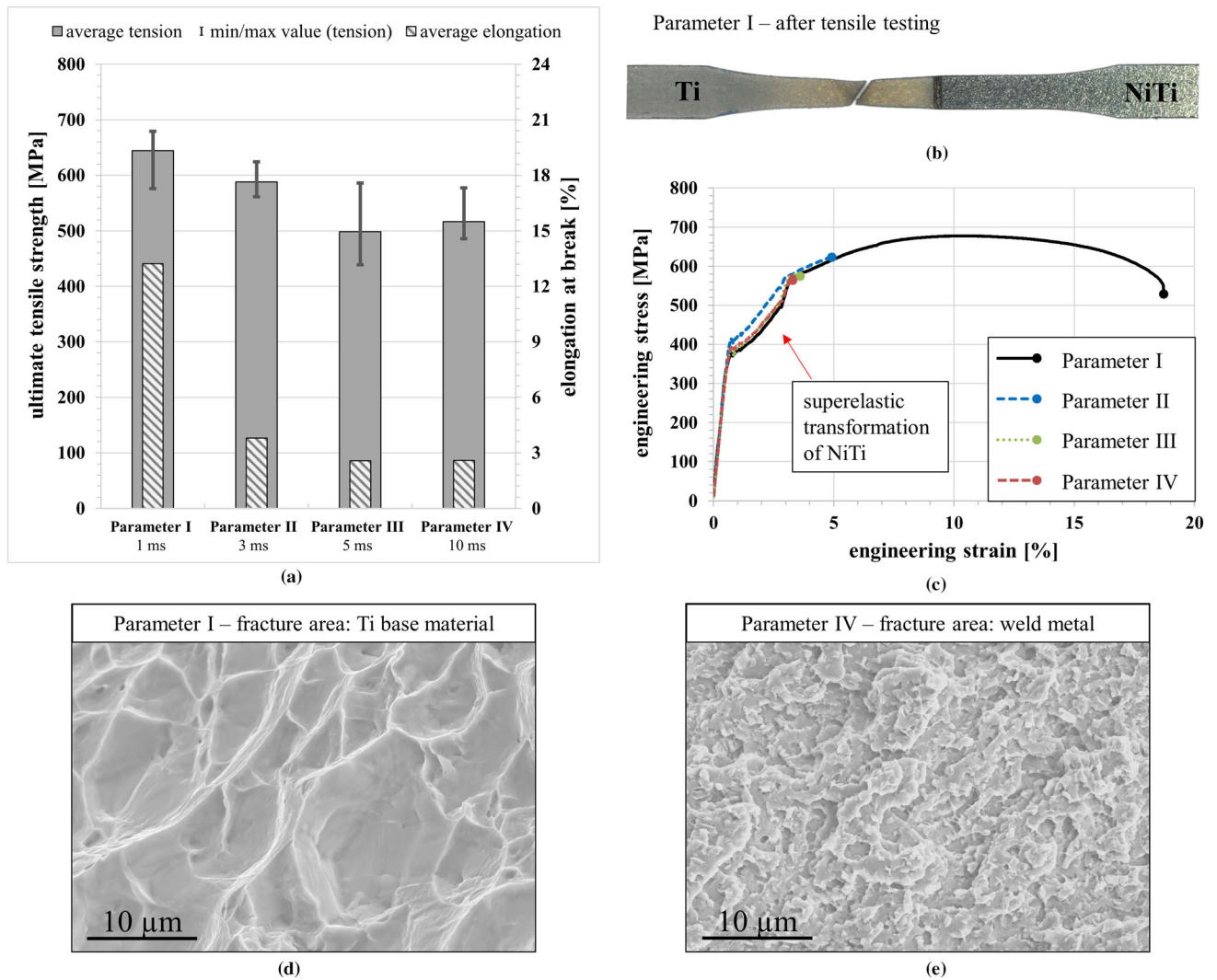


Fig. 10—(a) Data evaluation of the tensile tests for parameter set I to IV. (b) Macroscopic image of an exemplary specimen welded with parameter set I subsequent to tensile testing. (c) Engineering-stress-strain diagram of representative samples for each parameter set. (d) and (e) SEM fracture surface analyses.

microstructural evolution, in particular the accumulation of Ti- and Ni-rich interdendritic phases and the associated formation of IMC, consequently lead to an embrittlement of the joint. Nevertheless, despite the considerably degraded mechanical properties compared to parameter I, every investigated parameter set shows substantially improved mechanical properties compared to the majority of previous studies on Ti/NiTi dissimilar welded joints, either with or without the aid of filler materials.

Figure 10(c) shows an engineering stress-strain diagram with representative samples for each parameter set. It can be seen that all stress-strain curves flatten at a tensile stress of approximately 400 MPa and become significantly steeper again at 500 MPa. This concise progression is based on the stress-induced martensitic transformation of the NiTi base material, which occurs exactly in this stress range, as can be derived from Table III as well as Hellberg *et al.*,^[7] resulting in the characteristic superelastic plateau. While the samples of

parameter sets II, III, and IV fail shortly after the completion of the phase transformation, the specimen of parameter set I can fully utilize the superelastic plateau of the NiTi shape memory alloy and continue to withstand high strains up to 18.7 pct, proving an excellent ductility of the joint. However, in order to fully evaluate the superelastic properties of the welded material combination, further extensive mechanical analyses focusing on cycling loading are required. As shown in Figure 10(d), the corresponding fracture surface of parameter I shows ductile tensile dimples due to the high ductility of the titanium base metal, in which the fracture is localized. In contrast, the fracture morphology of parameter IV, which failed in the weld metal, differs significantly and represents an intergranular cleavage, which can be attributed to the limited ductility due to the expected increase in IMC formation mentioned above. This fracture behavior is also in good agreement with previous studies in which the specimens failed in the weld metal.^[25]

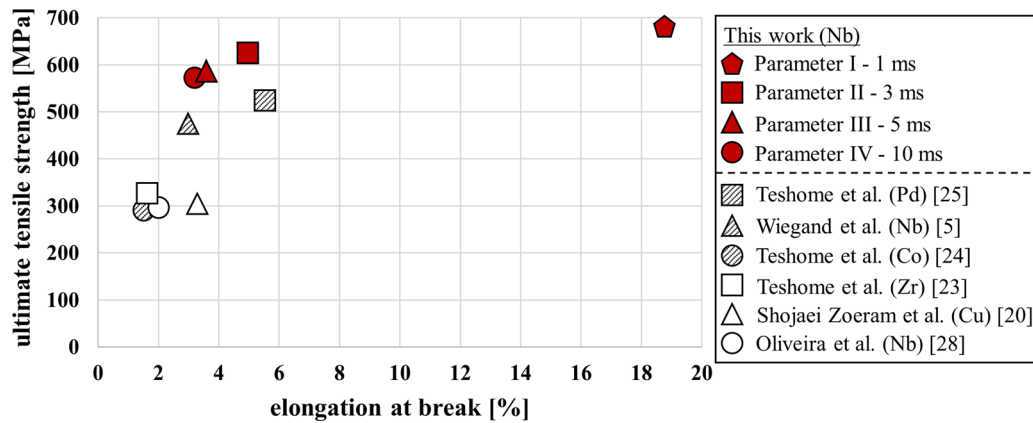


Fig. 11—Comparison of the maximum mechanical properties obtained in this work with the documented values of previous studies on dissimilar beam welding of titanium to NiTi using filler materials.

In addition to the excellent weldability, the mechanical analyses confirm that Nb is perfectly qualified as filler material for dissimilar joints of NiTi and Ti. In order to substantiate this statement, Figure 11 compares the mechanical properties obtained in this work with previous findings on dissimilar beam welding of titanium to NiTi using filler materials. Even compared to the very recent study by Teshome *et al.*,^[25] a significant increase in mechanical performance can be derived from this.

Based on the experimental results, it can be concluded that a short pulse duration, which correlates to a narrow weld seam width and a high proportion of Nb in the weld, leads to significantly improved mechanical properties of joints between Ti and NiTi, despite partly severe welding irregularities. In consideration of the determined low hardness values as well as the detailed comparison to parameter set IV by means of EDS and BSE, this observation confirms that the chemical composition exerts a superior influence on the mechanical properties of this dissimilar weld. The reproducibility, especially in the case of parameter set I, can certainly be increased by further optimization of the process parameters with a special emphasis on reducing the welding irregularities. Furthermore, a continuous beam welding process featuring a high-brilliance beam should be considered for future investigations, as it should be easier to obtain smaller weld seam widths with a sufficient binding of the three metals while omitting extensively high intensities on the workpiece surface. Moreover, inhomogeneous melting of the filler metal in-between pulses can be prevented.

V. CONCLUSION

In the investigation at hand, thin sheets of cp-Ti were joined to NiTi by means of pulsed laser beam welding with the aid of Nb as filler material. Different parameter sets with varying pulse durations were applied in order

to compare and evaluate the inherently deviating chemical compositions. The following main conclusions can be drawn from this study:

- Intermixing pure Nb into a Ti/NiTi-joint enables the fabrication of crack-free specimens in a reproducible manner using various process parameters, *e.g.*, different pulse durations and peak powers. Thus, the weldability is drastically increased compared to autogenous welding.
- Different pulse durations strongly affect the geometry and width of the weld seams and, consequently, the proportion of intermixed Nb.
- Short pulse durations of 1 ms lead to narrow weld seams with a high proportion of Nb that, however, are associated with severe welding irregularities, an inhomogeneous melting of the filler material and a bimodal grain size distribution.
- Longer pulse durations of 10 ms mitigate these irregularities, which in turn leads to a decrease of intermixed Nb and a higher area fraction of Ti- and Ni-rich phases, as confirmed by EDS and BSE analyses.
- Nanoindentation mappings as well as tensile tests revealed that shorter pulse durations and narrower weld seams lead to comparatively low hardness values and significantly improved ultimate tensile strengths, proving that a high content of Nb inside the weld seam is beneficial for dissimilar welding between Ti and NiTi.
- Superior mechanical performance was obtained by the shortest pulse duration of 1 ms, despite observed welding irregularities. Tensile specimens achieved ultimate tensile strength values of up to 679 MPa with a fracture in the unaffected Ti base material, which is undocumented in current literature.
- As these specimens can fully utilize the superelastic stress plateau of NiTi, the results offer enormous potential for future applications in manifold industries and overcome the previously known limitations of this

material combination, thus representing a substantial improvement of the current state-of-the-art in dissimilar welding of Ti to NiTi.

AUTHOR CONTRIBUTION

MW contributed to conceptualization, writing, project administration, investigation, and data evaluation. NS contributed to review and editing and investigation. LM contributed to review and editing, investigation. SB contributed to review and editing, supervision and validation, and funding acquisition.

FUNDING

Open Access funding enabled and organized by Projekt DEAL. The shown results were achieved in the project “Artfremdes Mikro-Strahlschweißen von Titan mit Nitinol und nichtrostenden Stählen zur Herstellung eines biokompatiblen Materialverbunds unter Verwendung von Zusatzwerkstoffen (MeTiWeld)” (reference IGF 21.601 N), which is supervised by the Forschungsvereinigung Schweißen und verwandte Verfahren e.V. of the German Welding Society and funded by the German Federation of Industrial Research Associations (AiF) by means of the Federal Ministry for Economic Affairs and Climate Action (BMWK) on the basis of a decision by the German Bundestag.

CONFLICT OF INTEREST

On behalf of all authors, the corresponding author states that there is no conflict of interest.

OPEN ACCESS

This article is licensed under a Creative Commons Attribution 4.0 International License, which permits use, sharing, adaptation, distribution and reproduction in any medium or format, as long as you give appropriate credit to the original author(s) and the source, provide a link to the Creative Commons licence, and indicate if changes were made. The images or other third party material in this article are included in the article's Creative Commons licence, unless indicated otherwise in a credit line to the material. If material is not included in the article's Creative Commons licence and your intended use is not permitted by statutory regulation or exceeds the permitted use, you will need to obtain permission directly from the copyright holder. To view a copy of this licence, visit <http://creativecommons.org/licenses/by/4.0/>.

REFERENCES

1. D.J. Hartl and D.C. Lagoudas: *Proc. Inst. Mech. Eng. Part G*, 2007, vol. 221, pp. 535–52.
2. J. MohdJani, M. Leary, A. Subic, and M.A. Gibson: *Mater. Des.* (1980–2015), 2014, vol. 56, pp. 1078–13.
3. L. Petrini and F. Migliavacca: *J. Metall.*, 2011, vol. 2011, pp. 1–5.
4. S. Saadat, J. Salichs, M. Noori, Z. Hou, H. Davoodi, I. Bar-on, Y. Suzuki, and A. Masuda: *Smart Mater. Struct.*, 2002, vol. 11, pp. 218–29.
5. M. Wiegand, L. Marks, N. Sommer, and S. Böhm: *Weld World*, 2022, vol. 67(1), pp. 77–88.
6. B. Li, L. Wang, B. Wang, D. Li, J.P. Oliveira, R. Cui, J. Yu, L. Luo, R. Chen, Y. Su, J. Guo, and H. Fu: *Mater. Sci. Eng. A*, 2022, vol. 843, 143135.
7. S. Hellberg, J. Hummel, P. Krooß, T. Niendorf, and S. Böhm: *Weld World*, 2020, vol. 64, pp. 2159–68.
8. C. Veiga, J.P. Davim, and A. Loureiro: *Rev. Adv. Mater. Sci.*, 2012, vol. 32, pp. 133–48.
9. P. Kah, M. Shrestha, and J. Martikainen: *AMM*, 2013, vol. 440, pp. 269–76.
10. M.M. Quazi, M. Ishak, M.A. Fazal, A. Arslan, S. Rubaiee, A. Qaban, M.H. Aiman, T. Sultan, M.M. Ali, and S.M. Manladan: *Opt. Laser Technol.*, 2020, vol. 126, 106090.
11. T. Deepan Bharathi Kannan, T. Ramesh, and P. Sathiya: *JOM*, 2016, vol. 68, pp. 1227–45.
12. A. Ascari, E.P. Zapico, V. Dimatteo, and A. Fortunato: *Procedia CIRP*, 2022, vol. 111, pp. 770–73.
13. G.R. Joshi, V.J. Badheka, R.S. Darji, A.D. Oza, V.J. Pathak, D.D. Burduhos-Nergis, D.P. Burduhos-Nergis, G. Narwade, and G. Thirunavukarasu: *Materials (Basel, Switzerland)*, 2022, vol. 15, p. 7234.
14. B. Ma, X. Gao, Y. Huang, P.P. Gao, and Y. Zhang: *Opt. Laser Technol.*, 2023, vol. 167, 109721.
15. C.A.F. Salvador, E.L. Maia, F.H. Costa, J.D. Escobar, and J.P. Oliveira: *Sci. Data*, 2022, vol. 9, p. 188.
16. H. Hermawan, D. Ramdan, and J. R. P. Djuansjah: *Biomedical Engineering - From Theory to Applications*, Ed. by R. Fazel, InTech, 2011.
17. M. Peters, J. Kumpfert, C.H. Ward, and C. Leyens: *Adv. Eng. Mater.*, 2003, vol. 5, pp. 419–27.
18. L. Hu, Y. Xue, and F. Shi: *Mater. Des.*, 2017, vol. 130, pp. 175–82.
19. S. Datta, M.S. Raza, S. Kumar, and P. Saha: *Adv. Mater. Process. Technol.*, 2018, vol. 4, pp. 614–25.
20. A. Shojaei Zoeram and S. Akbari Mousavi: *Mater. Des.*, 2014, vol. 61, pp. 185–90.
21. Z. Sun and J.C. Ion: *J. Mater. Sci.*, 1995, vol. 33(3), pp. 4205–14.
22. R.M. Miranda, E. Assunção, R.J.C. Silva, J.P. Oliveira, and L. Quintino: *Int. J. Adv. Manuf. Technol.*, 2015, vol. 81, pp. 1533–538.
23. F.B. Teshome, B. Peng, J.P. Oliveira, and Z. Zeng: *Mater. Manuf. Process.*, 2022, vol. 17, pp. 1942–954.
24. F.B. Teshome, B. Peng, J.P. Oliveira, S. Ao, W. Ke, F. Ge, and Z. Zeng: *J. Mater. Eng. Perform.*, 2022, vol. 31, pp. 9777–790.
25. F.B. Teshome, B. Peng, J.P. Oliveira, J. Shen, S. Ao, H. Li, L. Chen, C. Tan, X. Song, N. Zhou, and Z. Zeng: *Mater. Des.*, 2023, vol. 228, 111845.
26. J.L. Murray: *Bull. Alloy Phase Diagr.*, 1981, vol. 2, pp. 55–61.
27. M.J. Torkamany, F. Malek Ghaini, and R. Poursalehi: *Mater. Des. (1980–2015)*, 2014, vol. 53, pp. 915–20.
28. J.P. Oliveira, B. Pantoni, Z. Zeng, C.M. Andrei, Y. Zhou, R.M. Miranda, and F.B. Fernandes: *Acta Mater.*, 2016, vol. 105, pp. 9–15.
29. F. Ge, B. Peng, J.P. Oliveira, W. Ke, F.B. Teshome, Y. Li, and Z. Zeng: *Metals*, 2021, vol. 11, p. 1578.
30. NDC® Nitinol Devices & Components, Superelastic Nitinol Alloys - Material Data Sheet. <https://confluentmedical.com/wp-content/uploads/2016/01/Material-Data-Sheet-Superelastic.pdf>. Accessed 15 Mar 2023.
31. WHS Sondermetalle GmbH & Co. KG, Datenblatt Niob (Nb, NbZr1). <https://www.whs-sondermetalle.de/images/pdf/Nb-Niob.pdf>. Accessed 15 Mar 2023.
32. METALCOR GmbH, Datenblatt: Titan-Grade 4 (3.7065). <http://www.metalcor.de/datenblatt/124/>. Accessed 15 Mar 2023.
33. N. Sommer, F. Stredak, M. Wiegand, and S. Böhm: *Weld World*, 2023, vol. 67, pp. 51–62.
34. M. Čalkovský, E. Müller, and D. Gerthsen: *J. Microsc.*, 2023, vol. 289, pp. 32–47.

35. K.P. Gupta: *J Phys Equil and Diff*, 2008, vol. 29, pp. 194–97.
36. T. Guangxiang, G. Na, Z. Ming, L. Xionggang, Z. Jieyu, W. Guangxin, and L. Chonghe: TMS2013 Supplemental Proceedings, Ed. by TMS, John Wiley & Sons, Inc, Hoboken, NJ, 2013, pp. 361–70.

Publisher's Note Springer Nature remains neutral with regard to jurisdictional claims in published maps and institutional affiliations.